BL2B2

Photofragmentation of C_{60} in Valence Ionization

J. Kou[a], T. Mori[a], Y. Haruyama[b], Y. Kubozono[b] and K. Mitsuke[a,c]

[a]*Department of Vacuum UV Photo-Science, The Institute for Molecular Science, Myodaiji, Okazaki 444-8585, Japan*

[b]*Department of Chemistry, Faculty of Science, Okayama University, Okayama 700-8530, Japan*

[c] *Graduate University for Advanced Studies, Myodaiji, Okazaki 444-8585, Japan*

It is well-known that dissociative ionization of C_{60} results in fragment ions with even numbered carbon atoms (C_{60-2m}^{q+}, m=1,2,…). Experiments of laser multiphoton ionization[1] or electron impact ionization[2] have shown that these ions are produced via thermal fragmentation of C_{60} parent ions in highly excited vibrational states. Single photon excitation with a tunable synchrotron radiation is expected to be helpful in measuring the appearance energies of the fragment ions and investigating redistribution of internal energy of the parent ions, since one can estimate the magnitude of the vibronic energy initially deposited in the C_{60} system. However, no photoion yield curves for production of the fragment ions have been reported. As part of our recent studies on photoionization of fullerenes[3], we have measured the photoion yield curves of the fragment ions produced from C_{60} at $h\nu$ = 25 -150 eV to investigate mechanism of the photofragmentation of C_{60}.

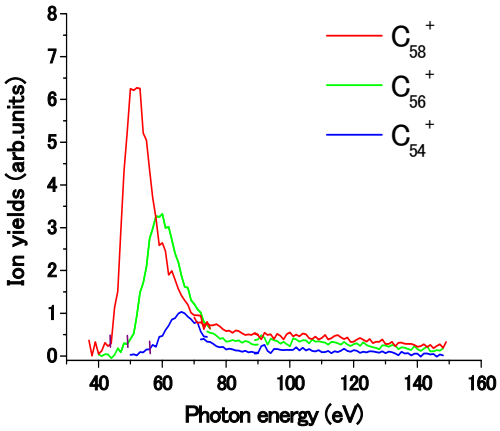

Fig. 1. Photofragment ion yields.

Yield curves for singly charged fragment ions are shown in Fig. 1. As the fragment ions become smaller, their appearance photon energies (AE) shift to higher energy side and curves rise more gently towards the peaks. All curves have long tails and a yield ratio of C_{58}^+: C_{56}^+: C_{54}^+ keeps a constant value of approximately 4: 3: 1 at $h\nu \geq$ 90 eV. The maximum internal energy (Ei_{max}) of the parent ion produced via an excitation with the appearance photon energy is found by

$$Ei_{max} = AE + Ev - Ip.$$

Here Ev = 3.3 eV means the initial vibrational energy deposited in C_{60} at a heating temperature of 680 K applied to produce a C_{60} molecular beam and Ip = 7.6 eV the ionization potential of C_{60}. We obtained Ei_{max} = 39.7±1, 44.7±1, and 51±1 eV for C_{58}^+, C_{56}^+, and C_{54}^+, respectively. These large internal energies are far beyond the adiabatic energies (E_0) for dissociation of $C_{60-2n}^+ \rightarrow C_{60-2n-2}^+ + C_2$ (n = 0,1,2,…)……(1).

We applied the RRKM model to estimate the internal energies of the parent ions. The detail of the calculation is the same as that described in Ref [2]. Fig. 2 shows yield distribution of C_{58}^+, C_{56}^+, and C_{54}^+ as a function of the internal energies of the parent ions. We adopted E_0 of 7.06, 6.78, and 6.60 eV for n =1, 2, and 3 in the reaction (1), respectively[2]. The internal energies for appearance thresholds of C_{58}^+, C_{56}^+, and C_{54}^+ are 40.7, 47.3, and 51.7 eV, respectively. These values are in good agreement with the observed Ei_{max}. However, all curves in the calculation lie in a range from 40 to 70 eV and do not reproduce the long tails in the higher energy side. Minimum photon energy for the excitation to this internal energy range is $44.3 \leq h\nu \leq 74.3$ eV. Therefore, the long tails observed at $h\nu \geq$ 90 eV indicate that photoelectron takes away a part of the excitation energy as a kinetic energy and leads to a production of the parent ion with an internal energy from 40 to 70 eV.

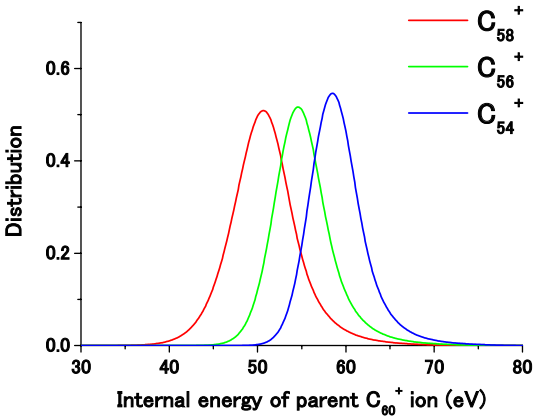

Fig.2 Distribution of fragment ions calculated with the RRKM model.

[1] P. Wurz and K. R. Lykke, J. Phys. Chem. **96,** 10129 (1992).

[2] R. Wörgötter, B. Dünser, P. Scheier, T. D. Märk, M. Foltin, C. E. Klots, J. Laskin, and C. Lifshitz,M. J. Chem. Phys. **104,** 1225 (1996).

[3] J. Kou, T. Mori, S. V.K. Kumar, Y. Haruyama, Y. Kubozono, and K. Mitsuke, J. Chem. Phys. **120,** 6005 (2004).

BL2B2

Absolute Photoabsorption Cross Section of C_{60}

T. Mori, J. Kou, Y. Haruyama*, Y. Kubozono*, K. Mitsuke

Department of Vacuum UV photo-science, Institute for Molecular Science, Okazaki 444-8585 Japan

**Department of Chemistry, Faculty of Science, Okayama University, Okayama 700-8530 Japan*

Relative photoabsorption cross sections of C_{60} have been reported by several groups. Most of the authors focused their attention to photon energies below 25 eV or those around the carbon 1s edge (~ 280 eV). Furthermore, only a few experiments have been made on the absolute photoabsorption cross section σ_{abs} of C_{60}. The σ_{abs} curve can be estimated by direct absorption of synchrotron radiation in a cell filled with C_{60} vapor. Jaensch and Kamke measured σ_{abs} by using this method in the vacuum UV region [1]. They were confronted with several serious problems. First, the available energy range is crucially restricted by the material of the windows of the cell. Good transmission should be secured for the windows up to the highest photon energy of interest even at high ambient temperatures. Second, knowing the sample number density is prerequisite for calculating σ_{abs}, though the density is markedly unstable at high temperatures. With these difficulties, there has been no report on σ_{abs} at photon energies above 24.5 eV, where only relative absorption cross sections have been determined from the yields of positive ions produced from C_{60} [2,3].

In this report, we attempt to obtain the σ_{abs} curve of C_{60} from 25 to 180 eV by means of mass spectrometry. For this purpose, several essential devices have been exploited in combination with a high-temperature source of gaseous fullerenes: a grazing-incidence monochromator, a conical nozzle, a quartz-oscillator thickness monitor, and an efficient time-of-flight (TOF) mass spectrometer. The thickness monitor was used for the measurement of the C_{60} density. The detail of the apparatus has been described elsewhere [4].

We obtained the σ_{abs} curve by following equation.

σ_{abs} = (Ion count rate)/{(Photon flux)·(The sample density)·(Interaction length)·(Sensitivity of the spectrometer)·(Residence time)·(Pulse frequency)}

A pulse voltage rising from the ground level to +100 V was applied to the ion repeller electrode as start trigger for the TOF measurement. The duration and frequency of this pulse voltage were 5 μs and 5 kHz, respectively. Ions were drawn through a central hole 10 mm in diameter of the grounded extractor electrode. Photoions were detected with a microchannel plate (MCP) electron multiplier. The Photon flux was measured by a photodiode.

The vapor of the fullerene was discharged from the nozzle with a throat diameter of 0.5 mm and a diverging angle of 7.2 degree. The distance between the throat of the nozzle and the central point of the ionization region was set to 34.8 mm. The number density at the photoionization region is obtainable from the sublimation rate, beam size there (18.5 mm^2), and the average of vertical velocity $\bar{v}$ of the C_{60} beam at the oven temperature T:

$$\bar{v} = \frac{1}{2} \cdot \sqrt{(8k_B \cdot T)/(\pi \cdot m)}$$

Where k_B is the Boltzmann constant and m is the mass of C_{60}. Assuming that the sublimation rate was 5 ng s^{-1} at T = 743.15 K, the number density is estimated from $\bar{v}$ = 74 m s^{-1} to be 0.765×10^9 molecules cm^{-3}.

The sensitivity of our spectrometer is derived from the signal counts of Kr whose absolute photoionization cross section is given in the literature [5].

The obtained cross section of C_{60} is shown in Fig. 1. The σ_{abs} reported by Kamke were found to agree well with our data at 24 eV. The reliability of the Kamke's data appears to be degraded to some extent at $h\nu$ >25eV.

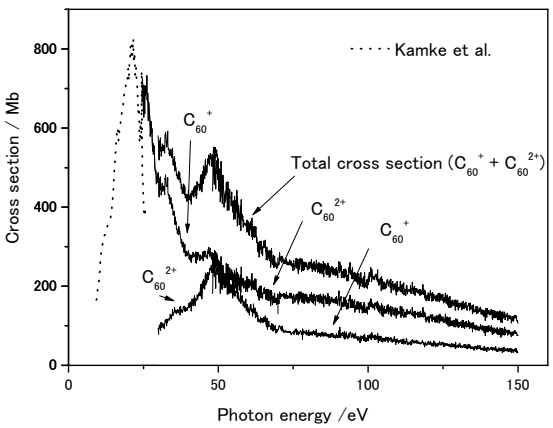

Fig. 1 Absolute cross section of C_{60}

[1] R. Jaensch and W. Kamke, Mol. Mat. 13, 143 (2000).
[2] I. V. Hertel et al. Phys. Rev. Lett. 68, 784 (1992)
[3] J. Kou et al. Chem. Phys. Lett. 374, 1 (2003)
[4] T. Mori et al. Rev. Sci. Inst., 74(8) 3769 (2003)
[5] J. A. R. Samson and W. C. Stolte, J. Electron Spectrosc. Relat. Phenom. 123, 265 (2002).

BL3B

Autoionization and Neutral Dissociation of Superexcited HI Studied by Two-Dimensional Photoelectron Spectroscopy

Y. Hikosaka and K.Mitsuke*

UVSOR Facility, Institute for Molecular Science, Okazaki 444-8585

**Department of Vacuum UV Photoscience, Institute for Molecular Science, Okazaki 444-8585*

Superexcited states, which are defined as neutral states lying in ionization continua, occupy considerable amounts of oscillator strength in the extreme ultraviolet region of a molecule. Autoionization induced by interelectronic interaction is their major decay processes. However, in the case of molecular superexcited states with relatively narrow autoionization widths, other processes such as neutral dissociation compete with autoionization and have sizable fractions in the decay.

Hydrogen halides are one of the classes of molecules whose superexcited states attract considerable attention in the literature. As for HCl and HBr, series of Rydberg states converging to the ionic $A\,^2\Sigma^+_{1/2}$ states appear as extensive vibrational progressions on photoabsorption spectra. Characters of the involving states and branching ratios have been well accounted for from both experimental and theoretical sides. In contrast, less information has been gained on decay from the corresponding Rydberg states of HI, since the Rydberg states do not exhibit distinct vibrational progressions but broad and almost structureless features on photoabsorption and photoionization spectra. Even for the superexcited states with such broad profiles, two-dimensional photoelectron spectroscopy, in which the photoelectron yield is represented as a function of both photon energy $E_{h\nu}$ and electron kinetic energy E_k, may offer information on the decay dynamics. This is because, when the photon energy is tuned to a superexcited state, the vibrational distribution of the final ionic state on the photoelectron spectrum is closely related to the potential energy surface of this autoionizing state. In addition, photoelectron spectroscopy can probe neutral dissociation of the superexcited state if the neutral fragments undergo autoionization.

Figure 1(a) shows a two-dimensional photoelectron spectrum (2D-PES) of HI measured in the $E_{h\nu}$ region of 11.10 - 14.85 eV. The $E_{h\nu}$ region encompasses the Franck-Condon gap between the $X^2\Pi$ and $A^2\Sigma^+_{1/2}$ states of HI^+. Hence, the 2D-PES is expected to show the features arising from the decay of the Rydberg states $HI^*(R_A)$ converging to $HI^+(A^2\Sigma^+_{1/2})$. Two intense diagonal stripes at $\Delta E \equiv E_{h\nu} - E_k$ = 10.39 and 11.05 eV result from the formation of spin-orbit components of the $v^+ = 0$ level of $HI^+(X^2\Pi)$. In several $E_{h\nu}$ regions extensive vibrational excitation of $HI^+(X^2\Pi)$ up to $v^+ \sim 12$ are noticeable. A broad diagonal pattern spreading around ΔE = 14 - 14.5 eV is ascribed to the formation of the $HI^+(A\,^2\Sigma^+_{1/2})$ state.

Figure 1(b) represents the curve obtained by summing electron counts over the whole E_k range as a function of $E_{h\nu}$. A broad peak centered at $E_{h\nu} \sim$ 12.3 eV can be seen on the curve. In analogy to HBr, this broad peak can be assigned to $5d\pi$ $HI^*(R_A)$ state. The 2D-PES exhibits strong vibrational excitation of $HI^+(X^2\Pi)$ over an $E_{h\nu}$ region from ~12 to 13.7 eV, which is attributable to autoionizing feature of the $5d\pi$ $HI^*(R_A)$ state [1]. In addition to the patterns due to molecular ionization, vertical stripes running parallel to the photon energy axis can be seen around ΔE = 13.5 - 14 eV. They are assigned as resulting from autoionization of the atomic Rydberg states $I^*[R(^3P_{0,1})]$ converging to $I^+(^3P_0$ or $^3P_1)$. The overall reaction scheme for the formation and autoionization of the iodine atom is described as follows [1]:

$$HI(X^1\Sigma^+) + h\nu \rightarrow HI^*(R_A) \quad (1a)$$

$$HI^*(R_A) \rightarrow HI^*[R(^4\Pi_{1/2})] \quad (1b)$$

$$HI^*[R(^4\Pi_{1/2})] \rightarrow H(^2S_{1/2}) + I^*[R(^3P_{0,1})] \quad (1c)$$

$$I^*[R(^3P_{0,1})] \rightarrow I^+(^3P_2) + e^- . \quad (1d)$$

In process (1d) the electron kinetic energy is definitely determined by the energy difference between atomic energy levels of $I^*[R(^3P_{0,1})]$ and $I^+(^3P_2)$, and independent of the initial excitation energy in process (1a). As a consequence, autoionization of $I^*[R(^3P_{0,1})]$ should give rise to vertical stripes running parallel to the $E_{h\nu}$ axis on the 2D-PES.

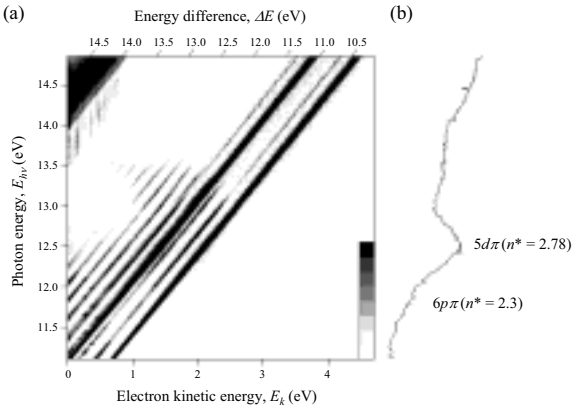

Fig. 1 (a) Two-dimensional photoelectron spectrum of HI in $E_{h\nu}$ = 11.10 - 14.85 eV. The electron yield, measured as a function of both $E_{h\nu}$ and E_k, is presented by the plots with eight tones from light to dark on a linear scale. Diagonal lines attached on the top of this figure denote the energy difference defined by $\Delta E = E_{h\nu} - E_k$. (b) The curve obtained by summing electron counts over the whole range of E_k as a function of $E_{h\nu}$.

[1] Y. Hikosaka and K. Mitsuke, J. Chem. Phys. submitted.

BL4B

A Toroidal Electron Analyzer for Observing Anisotropic Electron Emissions Following Molecular Inner-Shell Photoabsorption

Y. Hikosaka and E. Shigemasa
UVSOR Facility, Institute for Molecular Science, Okazaki 444-8585

Molecular inner-shell photoabsorption processes leading to both discrete and continuum states are intrinsically anisotropic, since an anisotropic orientational distribution of molecules is determined by the orientation of the transition dipole moment relative to the electric vector of the light. This anisotropy is reflected in the angular distribution of the products created either from the initial core hole state or from states following the rapid decay. Processes like photoelectron emission, Auger electron ejection, fluorescence, and photodissociation, all bear the vestige of the symmetry of the initial excited state.

An electron analyzer with toroidal shapes is one of the most suitable analyzers to observe the anisotropic electron emissions, owing to the simultaneous multi-energy and multi-angle detection with a reasonably-high energy-resolution. Recently, a "double toroidal" electron analyzer, which has been originally developed by a French group [1], has been constructed. The analyzer consists of a four element electrostatic conical lens and two toroidal deflectors connected, as illustrated in Fig. 1. The conical symmetry of the lens system limits the detection angle of electrons to 54.7° with respect to the cylindrical symmetry axis of the analyzer. The incident electrons are focused by the lens, and then dispersed in energy between the double toroidal deflectors, and may reach a delay-line-type imaging detector (Siegmund Scientific) mounted on the output plane. The imaging detection without any exit slit enables us to observe electrons within an energy range more than 10 % of the pass energy. Figure 2 shows an observed image for Kr $M_{4,5}N_{2,3}N_{2,3}$ Auger lines with kinetic energies in 50-57eV. The Auger lines are partially resolved, and accordingly four or more concentric circles are seen on the image. Since we set the cylindrical symmetry axis of the analyzer to be parallel to the electric vector of the incident radiation, no anisotropy should essentially be observed along the concentric circles. However, the concentric circles in Fig. 2 are, in practice, far from isotropy; particularly, a lack of intensity is detected at the top-right part of the image, which is due to a potential distortion by a gas nozzle. The other minor intensity modulations on the concentric circles are probably due to a transmission-efficiency fluctuation depending on angle. Actually the analyzer has three supporting struts in the lens system to keep its geometrical structure appropriate, which may induce insensitive areas on the detector.

The acceptance solid-angle of the analyzer is estimated to be about 6×10^{-2} sr. Such large acceptance angle is suitable to coincidence measurements. One of our plans is to combine this electron analyzer with an imaging analyzer for ion momentum observation. The coincidence setup would enable us to observe anisotropic electron emissions in molecular frame.

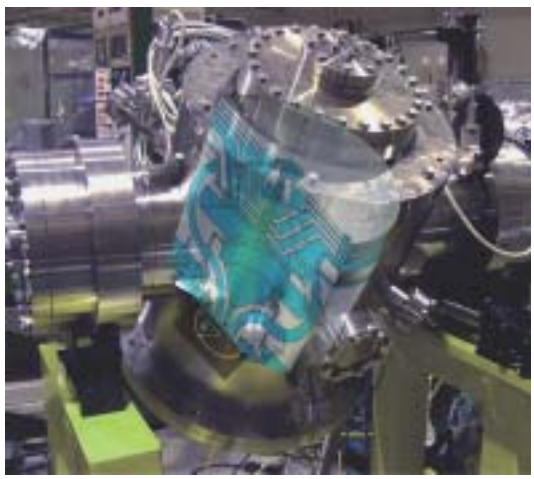

Fig. 1 A side view of the chamber with a schematic cutting image of the toroidal electron analyzer.

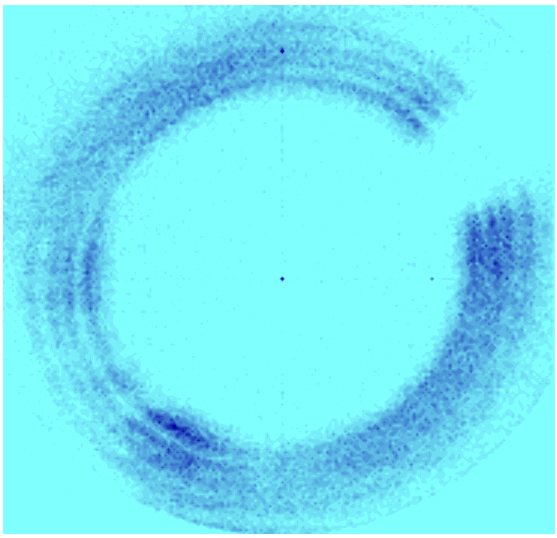

Fig. 2 An image observed by a delay-line-type imaging detector. The Kr $M_{4,5}N_{2,3}N_{2,3}$ Auger lines with kinetic energies in 50-57eV are partially resolved. A lack of intensity at the top-right part of the image is due to a potential distortion by the gas nozzle.

[1] C. Miron et al, *Rev. Sci. Instrum*. **68**, 3728 (1997).

BL4B

Observation of Vacuum Ultraviolet Fluorescence Following the N 1s Excitations of N_2O

Y. Hikosaka and E. Shigemasa
UVSOR Facility, Institute for Molecular Science, Okazaki 444-8585

Resonant Auger is the dominant decay process of molecular core-excited states. The dynamics of the resonant Auger transition, which is closely related to the electronic structure of the core-excited state, has received considerable attention, often in connection with state-specific fragmentation induced by core-excitation. Electron spectroscopy is the standard means to investigate Auger final-states accessed from each core-excited state, and many interesting findings such as lifetime/vibrational interference, detuning effects, fragmentation dynamics etc., have been studied in great detail.

When the Auger final-states have sufficient internal energies, fluorescence may be emitted from either the molecular ions or fragments formed through dissociations of the molecular ions. The ultraviolet fluorescence may be a unique probe for identifying the multielectron processes such as double excitations in the core ionization continua, because it is expected that such processes may lead to highly-excited molecular ions, fragment ions, and neutral fragments produced after the Auger decays.

We have constructed a 0.3-m Seya-Namioka-type fluorescence spectrometer, for observing the vacuum ultraviolet fluorescence following the molecular inner-shell excitation. A photo of the spectrometer is shown in Fig. 1. The dispersed fluorescence is detected by a position sensitive detector composed of three microchannel plates and a resistive anode encoder, where the front microchannel plate is coated by CsI. The position sensitive detector enables us to observe the fluorescence spectrum with its spectral range about 300 Å simultaneously. The wavelength resolution is estimated to be about 5 Å.

As our first attempt, we have measured the vacuum ultraviolet fluorescence from N_2O at the N 1s excitation region. Figure 2 indicates dispersed fluorescence spectra at the incident photon energies of 401 and 424 eV, where the $\pi^*(N_t)$ and σ^* resonances lie, respectively. The wavelength region simultaneously-observed was set to 450-750 Å, though we did not calibrate the wavelength precisely; an error within a few tens of Å is anticipated in the wavelength scale of Fig. 2. Many fluorescence lines can be seen in the spectra. Most of the lines in the short wavelength region may be regarded as corresponding to the transitions between ionic states, probably the emissions from atomic fragment ions; however, at the present stage we do not attempt to assign the fluorescence lines, due to the anticipated error in the wavelength scale. The same fluorescence lines are observable in the two spectra, implying that the $\pi^*(N_t)$ and σ^* core-excited states result in producing the same fluorescing species. In contrast, the Auger final states following these two core-excited states should be quite different from each other, according to the electronic properties of the core-excited states. The present observation suggests that most of the fluorescing species are not the molecular Auger final states, but the excited fragments produced by the dissociations after the core-hole relaxations. One interesting aspect seen in Fig. 2 is that the intensity ratios of several peaks between the two spectra are apparently different: the peaks at 460 and 510 Å in the spectrum of 424 eV is stronger than those of 401 eV, while the peaks at 610 Å exhibit the opposite behavior. This reflects different Auger final-states accessed by the resonant Auger processes.

Fig. 1 A photo of the vacuum ultraviolet fluorescence spectrometer.

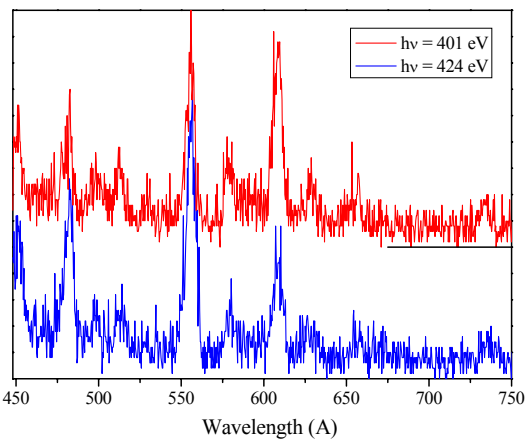

Fig. 2 Dispersed fluorescence spectra from N_2O measured at two different photon energies.